

# Nanoarchitectonics of Exfoliated Flexible Nanosheet Based on Laterally Stacked Macrocycles

Nano Shioda, Jung-Moo Heo, Bubsung Kim, Hiroaki Imai, Jong-Man Kim,\* and Yuya Oaki\*

2D nanostructures including monolayers and few layers exhibit unique properties originating from the anisotropic ultrathin nature. Conventional organic 2D nanostructures, such as covalent organic frameworks, are comprised of the planar  $\pi$ -conjugated macromolecules linked and extended parallel to the layers. The present work shows a new type of exfoliated organic 2D material. The macrocycles are stacked perpendicular to the lateral direction of the nanosheets. Self-assembly of a designed macrocyclic diacetylene monomer with a chair conformation forms the laminated structures containing the layers based on the perpendicularly arranged macrocycles. The exfoliable layered structures are obtained by the topochemical polymerization of the diacetylene moieties. The intercalation and subsequent swelling provide the nanosheets based on the laterally stacked macrocycles in aqueous phase. The colloidal nanosheets possess structural flexibility with the molecular motions originating from the ultrathin nature and conformational diversity. The hydrogel cross-linked with the flexible nanosheets exhibits unique stretching and thermoresponsive shrinking properties. The present work implies the potential of the flexible 2D materials based on the macrocycles.

Functional organic layered materials, such as layer-by-layer assembly and smectic liquid crystals, exhibit dynamic functions.<sup>[12–24]</sup> However, the exfoliation of these soft layered materials was not studied in the previous works. Although a couple of previous works showed intercalation of organic layered materials,<sup>[17–20]</sup> the exfoliation was not fully studied compared with inorganic materials.<sup>[21]</sup> Exfoliation of soft organic layered materials has the potentials for providing flexible nanosheets with dynamic molecular motion. In recent years, organic layered materials have been designed to obtain the exfoliated 2D structures containing functional molecules. For example, covalent and metal-organic frameworks (COFs and MOFs) with the layered structures are exfoliated into the nanosheets.<sup>[22–24]</sup> The resultant nanosheets are comprised of the planar  $\pi$ -conjugated macromolecules


## 1. Introduction

2D materials are obtained in a variety of inorganic and organic compounds.<sup>[1–5]</sup> The precursor layered materials are exfoliated into the nanosheets, such as monolayers and few layers.<sup>[6–11]</sup>

linked and extended parallel to the layers. These organic 2D materials are structurally rigid to induce the dynamic molecular motions because of the planar covalent networks without the conformational variety. The present work shows a new type of 2D polymer nanosheet comprised of the laterally stacked macrocycles (**Figure 1**). The molecular motion and conformational variety of the macrocycles have the potentials for providing the structural flexibility of the nanosheets (the orange arrows in **Figure 1a**). Here we showed nanoarchitectonics of macrocyclic diacetylene (MCDA), including the synthesis, controlled organization, polymerization, and exfoliation (**Figure 1**).

N. Shioda, H. Imai, Y. Oaki  
 Department of Applied Chemistry, Faculty of Science and Technology  
 Keio University  
 Yokohama 223-8522, Japan  
 E-mail: oakiyuya@applc.keio.ac.jp  
 J.-M. Heo, B. Kim, J.-M. Kim  
 School of Chemical Engineering  
 Hanyang University  
 Seoul 04763, South Korea  
 E-mail: jmk@hanyang.ac.kr

Diacetylene (DA) derivatives are used for syntheses of polydiacetylene (PDA) with stimuli-responsive color-change properties.<sup>[24–33]</sup> The adjacent DA moieties within a distance shorter than 0.5 nm are topochemically polymerizable in the self-assembled condensed states.<sup>[34]</sup> The tunable color-change and/or conductive properties of PDA have been extensively studied for sensing applications.<sup>[25–33,35–40]</sup> In recent years, ultrathin 2D nanostructures of PDA have been synthesized by bottom-up and top-down approaches.<sup>[41–44]</sup> Self-assembly of the specifically designed amphiphilic and macrocyclic DA monomers formed the colloidal nanosheets exhibiting the stimuli-responsive color-change properties.<sup>[42–44]</sup> Our group reported the exfoliation methods to obtain the PDA nanosheets consisting of the linear amphiphilic DA.<sup>[41]</sup> In the present work, the PDA

 The ORCID identification number(s) for the author(s) of this article can be found under <https://doi.org/10.1002/admi.202300521>

© 2023 The Authors. Advanced Materials Interfaces published by Wiley-VCH GmbH. This is an open access article under the terms of the Creative Commons Attribution License, which permits use, distribution and reproduction in any medium, provided the original work is properly cited.

DOI: 10.1002/admi.202300521

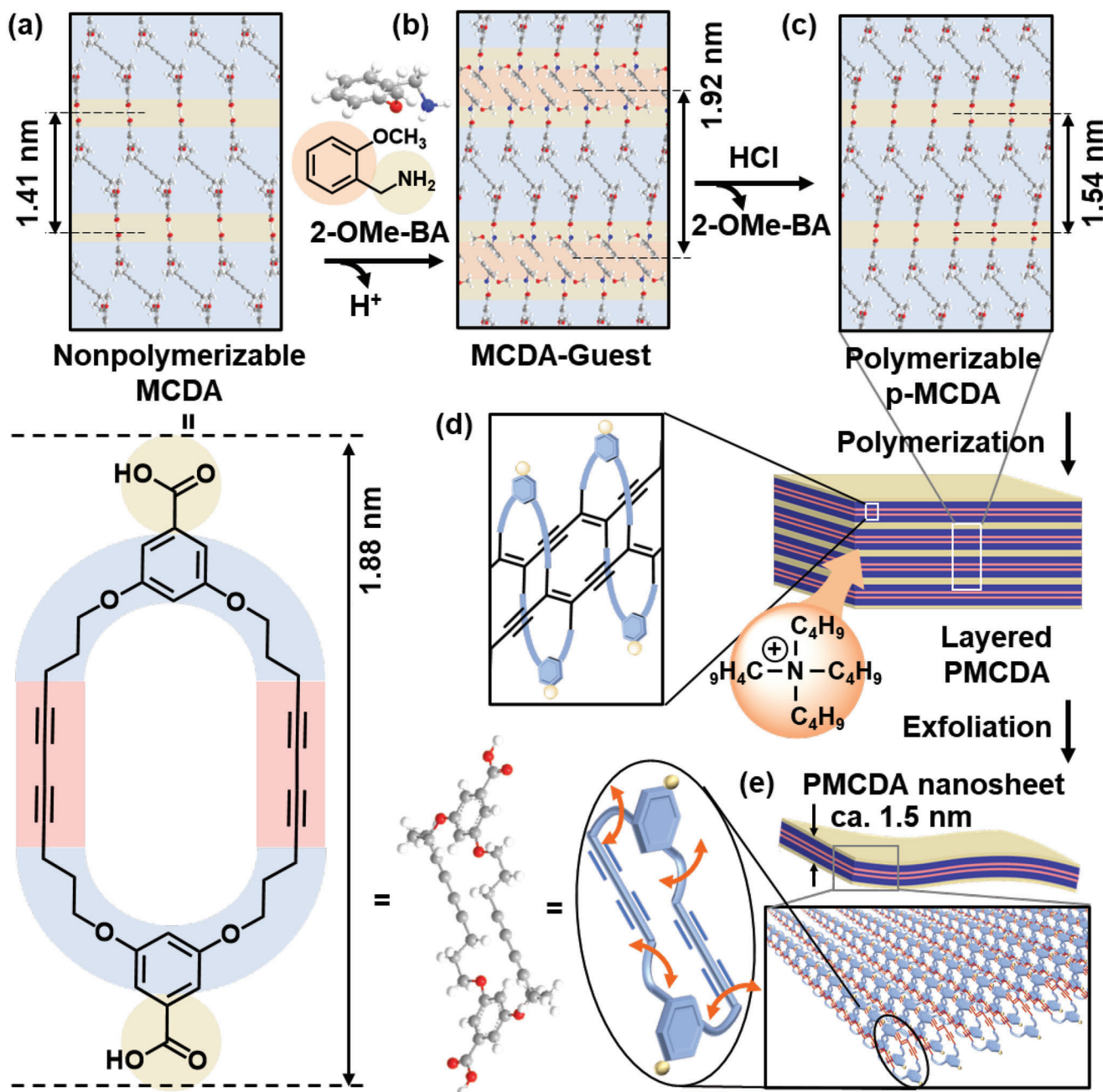


**Figure 1.** Schematic illustrations for the synthesis of the PMCDA nanosheets. a) Molecular structures of MCDA monomer and its nonpolymerizable layered crystal structure. b) MCDA-(2-OMe-BA) composites through the intercalation of 2-OMe-BA as a guest. c) p-MCDA obtained by the ion exchange to proton. d) Topochemical polymerization to PMCDA. e) PMCDA nanosheet through the exfoliation with intercalation of TBA<sup>+</sup> and osmotic swelling.

nanosheets based on MCDA were synthesized through exfoliation (Figure 1). The MCDA-based nanosheets have potential for exhibiting the structural flexibility with the conformational variety. The macrocycle-based PDA nanosheets were applied to not typical colorimetric sensing but forming the hydrogels as the cross-linker. The hydrogel showed the characteristic stretching and thermoresponsive volume-changing properties.

## 2. Results and Discussion

### 2.1. Synthesis of the Macrocycle-Based PDA Nanosheets

The nanosheets of the polymerized MCDA (PMCDA) were obtained through the ion-exchange, polymerization, and exfoliation processes (Figure 1). The MCDA monomer was synthesized and characterized in our previous works (Figure 1a).<sup>[45,46]</sup>

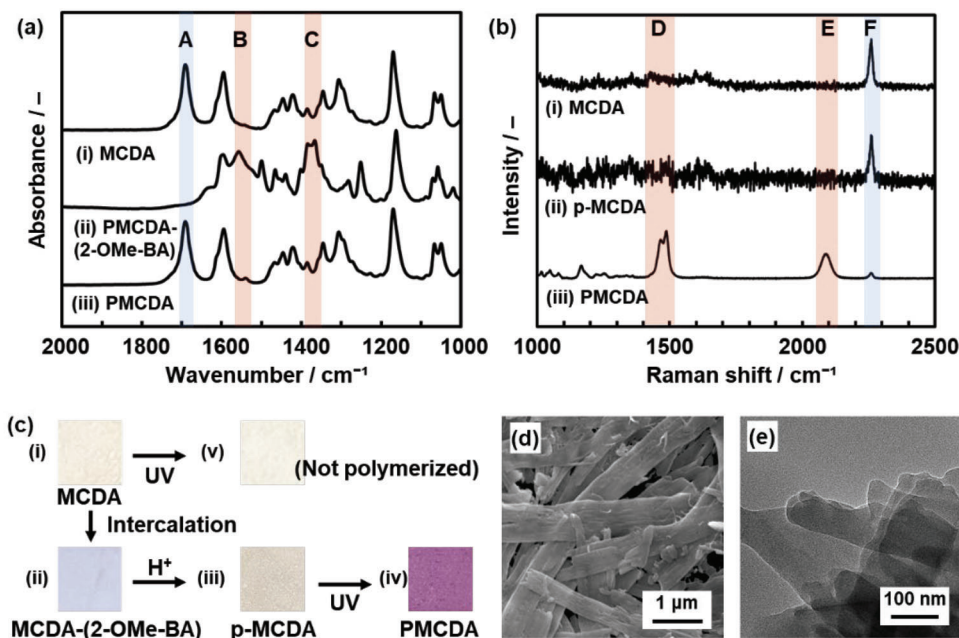


**Figure 2.** Precursor layered materials. a) FT-IR spectra of the original MCDA (i), MCDA-(2-OMe-BA) (ii), and p-MCDA (iii). b) Raman spectra of the original MCDA (i), p-MCDA (ii), and PMCDA (iii). c) Photographs of the powdered samples. d, e) SEM and TEM images of PMCDA, respectively.

The polymerized layered structure is required to inhibit the dislocation during the exfoliation in a dispersion medium. However, the layered structure of MCDA is not topochemically polymerized with the irradiation of UV light because the distance between the adjacent DA moieties is longer than 0.5 nm (Figure 1a). Our previous work showed that the intercalation of the guest molecules formed the topochemically polymerizable layered structure by shortening the distance between the DA moieties through the conformational changes (Figure 1b).<sup>[47]</sup> However, the exfoliation was not studied in the previous work. Here 2-methoxybenzylamine (2-OMe-BA) was used as a guest.<sup>[47]</sup> Then, the interlayer guest of MCDA-(2-OMe-BA) was exchanged to proton to obtain the topochemically polymerizable protonated layered MCDA (p-MCDA) (Figure 1c). The topochemical polymerization of p-MCDA formed the polymerized layered p-MCDA (PMCDA) containing the interlayer proton (Figure 1d). PMCDA was exfoliated into the nanosheets in an aqueous phase through the intercalation of bulky organic cation, i.e., tetrabutylammonium cation (TBA<sup>+</sup>), based on acid-based reaction and subsequent osmotic swelling with water (Figure 1e). The detailed procedure was described in the Supporting Information.

## 2.2. Formation of the Exfoliable Precursor Layered Material

The MCDA monomer showed the absorption  $\approx 1690\text{ cm}^{-1}$  corresponding to C=O stretching vibration of the dimerized carboxy group on Fourier-transform infrared (FT-IR) spectrum (band A of spectrum (i) in Figure 2a). All the other peaks were assigned to the structures of MCDA (Figure S1, Supporting Information). After the intercalation of 2-OMe-BA and polymerization (PMCDA-(2-OMe-BA)), the absorption  $\approx 1690\text{ cm}^{-1}$  disappeared (spectrum (ii) in Figure 2a), and the absorptions  $\approx 1570$  and  $1390\text{ cm}^{-1}$  orig-

inating from the carboxylate group appeared (bands B and C). PMCDA showed the same FT-IR spectrum as that of the original MCDA (spectra (i) and (iii) in Figure 2a). The interlayer distance ( $d_0$ ) characteristic of the layered structure was shifted from  $d_0 = 1.41$  to 1.92 nm with the intercalation of 2-OMe-BA on the X-ray diffraction (XRD) patterns (Figure S2, Supporting Information). The protonation directed the shift of  $d_0$  to 1.54 nm for PMCDA, even though the weaker peak  $d_0 = 1.41$  nm for the original MCDA remained (Figure S2, Supporting Information). The shift of  $d_0$  indicates that the tilted angle of the MCDA molecules in the layered structure  $48^\circ$  is changed to  $55^\circ$  with the conformational change (Figure 1a,c; Figure S2, Supporting Information). The change in the packing state of the MCDA molecules facilitates the topochemical polymerization by shortening the distance between the DA moieties. In our previous works, the similar MCDA molecules preserved the chair-like conformation in the organized states (Figure S2, Supporting Information).<sup>[45,48,49]</sup>

The monomeric MCDA and p-MCDA showed the peaks corresponding to C≡C bond of the DA moiety  $\approx 2250\text{ cm}^{-1}$  on the Raman spectra (band F of spectra (i) and (ii) in Figure 2b). After the polymerization of p-MCDA, the peaks  $\approx 1450$  and  $2100\text{ cm}^{-1}$  corresponding to the ene-yne structure were observed for PMCDA (bands D and E of spectrum (iii) in Figure 2b). PMCDA showed the purple color characteristic of PDA (panel (iv) in Figure 2c), whereas such coloration was not observed on the intermediates MCDA, MCDA-(2-OMe-BA), and p-MCDA (panels (i)–(iii) in Figure 2c). The original MCDA was not polymerized with the UV-irradiation (panels (i) and (v) in Figure 2c; Figure S3, Supporting Information). The Formation of PMCDA was supported by thermogravimetry (TG) and CHN elemental analyses (Figure S4, Supporting Information). Alternative to the above route, the red-color p-MCDA was obtained by the ion-exchange of PMCDA-(2-OMe-BA).

The average sizes of the PMCDA nanoribbons were  $0.49 \pm 0.18 \mu\text{m}$  for width,  $3.44 \pm 2.12 \mu\text{m}$  for length, and  $87.6 \pm 4.3 \text{ nm}$  for thickness on the images of scanning and transmission electron microscopy (SEM and TEM) (Figure 2d,e; Figure S5, Supporting Information). In this manner, the exfoliable PMCDA was obtained through the intercalation, ion exchange, and topochemical polymerization (Figure 1a–d).

### 2.3. Exfoliation into the PMCDA Nanosheets

PMCDA was exfoliated into the PMCDA nanosheets with the dispersion in an aqueous solution containing tetrabutylammonium hydroxide (TBAOH) at room temperature for 1 h (Figure 3). The transparent colloidal liquid showed orange color (the inset of Figure 3a). The PMCDA nanosheets  $14.7 \pm 5.8 \text{ nm}$  in the average lateral size (the sample number ( $n$ ) = 101) were observed as the white objects in black background by high-angle annular-dark field of scanning TEM (HAADF-STEM) (Figure 3a,c; Figure S6, Supporting Information). The anionic exfoliated nanosheets were collected on a silicon substrate coated with cationic polyethylenimine (PEI,  $M_n = 6.0 \times 10^4$ ) for the AFM observation (Figure S7, Supporting Information). The average thickness was  $4.8 \pm 7.3 \text{ nm}$  on the images of atomic force microscopy (AFM,  $n = 88$ ) (Figure 3b,d; Figure S7, Supporting Information). The curvature factor of a cantilever originating from the factory-default value and the deterioration with the use has an influence on the length scale of the AFM image in the lateral direction. The lateral size of the nanosheets has differences in the AFM and TEM images (Figure 3a–c). Therefore, in the present work, the lateral size was estimated not from the AFM images but from the TEM images. The exfoliation proceeds with the intercalation of  $\text{TBA}^+$  and subsequent osmotic swelling.<sup>[50,51]</sup> The thickness ( $t/\text{nm}$ ) of the PMCDA monolayer (the layer number ( $N_L$ ) = 1) is estimated to be  $\approx 2.5 \text{ nm}$  on the assumption that the sizes of MCDA and  $\text{TBA}^+$  are  $\approx 1.5$  and  $1.0 \text{ nm}$ , respectively (Figure S8, Supporting Information). The histogram of the thickness indicates the abundance ratio is 50.0% for the monolayers ( $N_L = 1$ ,  $1.0 < t \leq 2.5$ ), 36.4% for the few layers ( $N_L = 2-5$ ,  $2.5 < t \leq 12.5$ ), and 13.6% for the multilayers ( $6 \leq N_L$ ,  $12.5 < t$ ) (Figure 3d). The exfoliated anionic nanosheets in the aqueous colloid were collected with the addition of zinc acetate. The orange precipitate was observed on the bottom of the sample bottle (inset of Figure 3e). The flakes corresponding to the restacked nanosheets with zinc ion ( $\text{Zn}^{2+}$ ) were observed by SEM (Figure 3e; Figure S9, Supporting Information). These results indicate the formation of the exfoliated PMCDA nanosheets.

The photochemical properties were measured to study the structural flexibility of the PMCDA nanosheets compared with that of the other different PDA nanosheets. In the colloidal state, the differences in the flexibility can be observed in the UV–vis and photoluminescence spectra. PDA shows color changes in response to external stimuli, such as heat, light, and force.<sup>[25–33,35–40]</sup> The molecular motion induces the torsion of the PDA main chain by shortening the effective conjugation length. The color change in the macroscopic appearance originates from the change in the torsional angle of the PDA main chain in molecular level. UV–vis absorption peak has a correlation with the torsional angle of the PDA main chain (Figure S10, Supporting Information).<sup>[52,53]</sup> Our

intention here is to study the photochemical properties originating from the structural flexibility of the nanosheets (Figure 3f,g). As a reference, the rigid type of the layered PDA was prepared by the self-assembled linear rod-like amphiphilic DA monomer (PLDA), 10,12-pentacosadiynoic acid, and then exfoliated into the nanosheets under the same conditions (Figure S11, Supporting Information).<sup>[41]</sup> The original layered PMCDA and PLDA in the powdered state showed the broadened spectra with the absorption maxima  $\approx 570$  and  $670 \text{ nm}$ , respectively (Figure 3f). The exfoliated nanosheets in the colloidal state showed the shift of the absorption maxima to  $\approx 480 \text{ nm}$  for PMCDA and  $540 \text{ nm}$  for PLDA (Figure 3f). As another reference, PMCDA-(2-OMe-BA) with heating at  $230 \text{ }^\circ\text{C}$  showed a peak  $\approx 490 \text{ nm}$  similar to that of the exfoliated nanosheets. After the exfoliation, the UV–vis spectra were shifted to the shorter wavelength region. The PDA main chain is distorted by the dynamic molecular motion of the nanosheets dispersed in the liquid phase. Moreover, the spectrum of the exfoliated PMCDA nanosheets was located at the shorter wavelength region compared with the PLDA nanosheets. The PMCDA nanosheets have a more flexible structure ensuring the molecular motion compared with PLDA. The flexibility originates from the macrocyclic framework with the conformational diversity (Figure S10, Supporting Information). The interaction between  $\text{TAB}^+$  and PMCDA nanosheets has also effects on the color change with the exfoliation. The PMCDA and PLDA nanosheets showed the emission peaks  $\approx 570$  and  $579 \text{ nm}$  on the photoluminescent spectra, respectively (Figure 3g). The Stokes shift was calculated to be  $92 \text{ nm}$  for PMCDA and  $43 \text{ nm}$  for PLDA. This fact also implies the structural flexibility of PMCDA.

### 2.4. Hydrogel Based on PMCDA Nanosheets

The resultant PMCDA nanosheets were used as a cross-linker of poly(*N*-isopropylacrylamide) (PNIPAAm) hydrogel (Figure 4). Monomer *N*-isopropylacrylamide (NIPAAm), *N,N,N',N'*-tetramethylethylenediamine (TMED) as an accelerator, and potassium persulfate (KPS) as an initiator were dissolved in the aqueous colloid containing the PMCDA nanosheets. The hydrogel showed light yellow (Figure 4a). The two reference hydrogels were prepared using the different cross-linkers, namely the PLDA nanosheets exfoliated under the same conditions and a typical organic cross-linker *N,N'*-methylenebisacrylamide (MBAAm) (Figure 4b,c). In these samples, the molar ratio of the cross-linking site to the NIPAAm monomer was adjusted to 0.176%. When the concentration of the cross-linker was changed, the stretchable hydrogel was not obtained for both PNIPAAm-PMCDA and PNIPAAm-PLDA (Figure S12 in the Supporting Information).

The PNIPAAm-PMCDA hydrogel was stretched to the extension ratio ( $\lambda$ ) 44.0–52.8 times (the sample number  $n = 3$ ) and then fractured (Figure 4d,f; Figure S13, Supporting Information). On the other hand, the hydrogel containing PLDA nanosheets was stretched to  $\lambda = 3.6$ – $7.7$  ( $n = 3$ ) and then fractured (Figure 4d,e). The hydrogel cross-linked with MBAAm was fragile and broken during gripping by the jigs of the tester (the right panel in Figure 4c). The PNIPAAm-PMCDA hydrogel showed distinctive stretching properties compared with other reference gels. The PNIPAAm chain is cross-linked with the carboxy groups

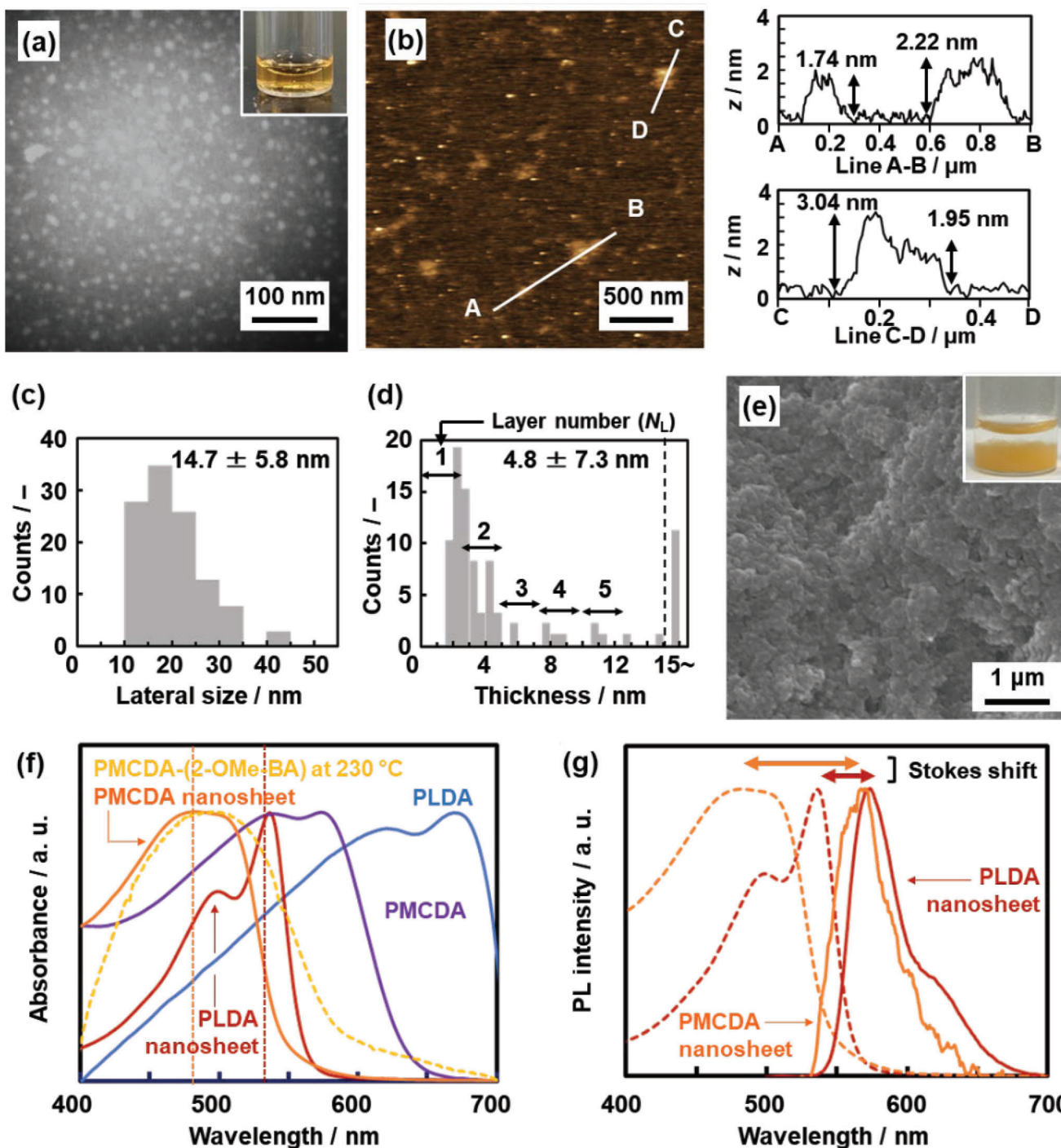


**Figure 3.** PMCDA nanosheets. a) HAADF-STEM image and photograph of the colloidal liquid (inset). b) AFM image with the height profiles. c,d) Histograms of the lateral size (c,  $n = 101$ ) and thickness (d,  $n = 88$ ) with the average sizes. e) SEM image of the restacked PMCDA nanosheets with zinc ion and photograph of the precipitate (inset). f) UV-vis spectra of the layered PLDA (blue) and PMCDA (purple) in the powdered state, their exfoliated PLDA (red) and PMCDA (orange) nanosheets, and PMCDA-(2-OMe-BA) with heating at 230 °C (yellow). g) UV-vis (dashed line) and photoluminescent (solid line) spectra of the PLDA (red) and PMCDA (orange) nanosheets.

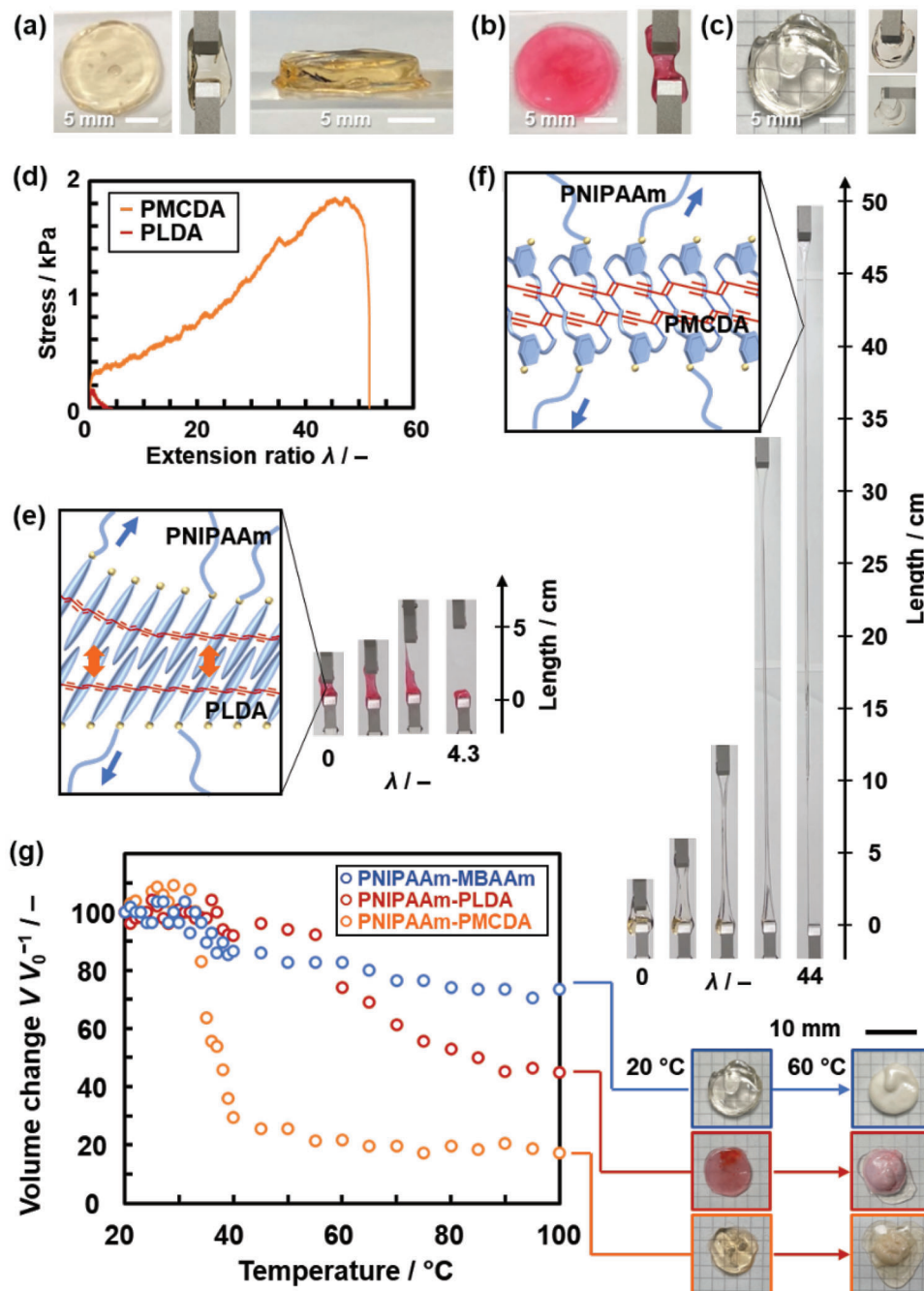


**Figure 4.** PNIPAAm hydrogels cross-linked by the PMCDA nanosheets, PLDA nanosheets, and MBAAm. a) Photographs of the PNIPAAm-PMCDA gel (left: top view, center: gripped by the jigs, and right: side view). b) Photographs of the PNIPAAm-PLDA gel (left: top view and right: gripped by the jigs). c) Photographs of a conventional PNIPAAm-MBAAm gel (left: top view and right: gripped by the jigs). d) Stress-strain curves of the PNIPAAm-PMCDA (orange) and PNIPAAm-PLDA (red) gels. e, f) Photographs (right panels) and schematic structure models (left panels) of the PNIPAAm-PLDA (e) and PNIPAAm-PMCDA (f) gels with stretching using tester, respectively. g) Relationship between temperature and  $V/V_0^{-1}$  for the thermoresponsive volume changes of the PNIPAAm-PMCDA (orange), PNIPAAm-PLDA (red), and PNIPAAm-MBAAm (blue) hydrogels (left) and the photographs at 20 and 60 °C (bottom right).

(COOH) on the surface of the PMCDA and PLDA nanosheets via the hydrogen bonding, whereas the covalent bond is formed with MBAAm. As the molar ratio of the cross-linking site to the monomer is constant for the three hydrogels, the nanosheets provide the spatially concentrated cross-linking sites on the sur-

face. In contrast, the cross-linking sites of MBAAm are dispersed throughout the hydrogel at molecular level. The nanosheets afford the longer stretching length of the PNIPAAm chains between the cross-linking sites compared with MBAAm. As the lateral size of the nanosheets was  $14.7 \pm 5.8$  nm for PMCDA

and  $91.8 \pm 50.5$  nm for PLDA (Figure 3a,c; Figure S11, Supporting Information), the longer distance between the cross-linking sites was prepared in the PNIPAAm-PLDA hydrogel. In fact, the PNIPAAm-PMCDAs hydrogel showed more stretchable properties (Figure 4e,f). The PLDA nanosheets have a lamellar structure based on the densely-packed amphiphilic DA molecules and their interlayer van der Waals interaction (the orange arrows in Figure 4g).<sup>[41]</sup> On the other hand, the PMCDAs nanosheets consist of the covalently linked macrocycles with a conformational variety. The structural stability and conformational variety of PMCDAs contribute to the stretching properties of the PNIPAAm chains on the assumption that the monolayered nanosheets are homogeneously dispersed in the hydrogel in the same states (Figure 4f). The lateral size, thickness, and dispersibility of the nanosheets can be actually involved in the stretching properties. In previous works, the similar highly stretchable hydrogels were obtained using inorganic clay nanosheets as the cross-linkers.<sup>[54,55]</sup> In the present work, the organic nanosheets enable the similar stretchable properties. If the blue-colored PMCDAs nanosheets are obtained even after the exfoliation process, it can be applied to prepare a variety of new sensing materials.

The PNIPAAm-PMCDAs gel showed the characteristic thermoresponsive volume changes (Figure 4g; Figure S14, Supporting Information). The gel samples were heated in the range of 20–40 °C by 1 K and in the range of 40–100 °C by 5 K. The PNIPAAm-PMCDAs gel was crowded  $\approx 27$  °C, whereas such crowding was observed in the range of 32–35 °C for the PNIPAAm-PLDA and 39–40 °C for PNIPAAm-MBAAm gels (Figure S14, Supporting Information). The volume of the gels shrank with increasing temperatures. The ratio ( $V/V_0^{-1}$ ) of the volume at a certain temperature ( $V$ ) to the initial volume at 20 °C ( $V_0$ ) was calculated from the photographs (Figure 4g; Figures S14 and S15, Supporting Information). The PNIPAAm-PMCDAs gel exhibited the largest thermoresponsive volume changes compared with the reference samples. The smaller PMCDAs nanosheets with the structural flexibility afford the large volume changes with the shrinkage of the gel through the aggregation of the PNIPAAm chains. In contrast, the larger PLDA nanosheets with the structural rigidity inhibit such aggregation of the PNIPAAm chains. In this manner, the conformational variety, structural stability, and flexibility of PMCDAs provide the unique properties of the hydrogel.

### 3. Conclusion

An organic 2D material based on the laterally stacked macrocycles was synthesized by the designed layered structure and its exfoliation. The intercalation, ion-exchange, and polymerization formed the exfoliable layered structure. The layered PMCDAs was exfoliated into the nanosheets through the intercalation of the bulky ions and osmotic swelling in aqueous media. The PMCDAs nanosheets were flexible compared with the PLDA nanosheets because of the conformational diversity of the macrocycles. The PNIPAAm hydrogel cross-linked with PMCDAs nanosheets showed the highly stretchable over the extension ratio 44.0. The characteristic thermoresponsive volume shrinkage was also observed with heating. If macrocycles containing a variety of functional molecular units are designed, similar flexible organic 2D materials can be obtained by exfoliation through the

formation of exfoliable layered structures. Macrocycle-based 2D materials can be applied as a nanoscale building block to obtain soft materials, such as liquid crystals, gels, and composites, with more flexible structures and dynamic functions.

### Supporting Information

Supporting Information is available from the Wiley Online Library or from the author.

### Acknowledgements

This work was supported by the JSPS-KAKENHI (JP22H02148 and JP22H04559) (Y.O.), the Asahi Glass Foundation, (Y.O.), and the NRF-Korea (2021R1A2C2005906 and 2021M3H4A1A02051834) (J.M.K.).

### Conflict of Interest

The authors declare no conflict of interest.

### Data Availability Statement

The data that support the findings of this study are available from the corresponding author upon reasonable request.

### Keywords

2D materials, exfoliation, layered structures, macrocycles, nanosheets

Received: June 19, 2023

Revised: July 31, 2023

Published online:

- [1] J. Sakamoto, J. van Heijst, O. Lukin, A. D. Schlüter, *Angew. Chem., Int. Ed.* **2009**, *48*, 1030.
- [2] V. Nicolosi, M. Chhowalla, M. G. Kanatzidis, M. S. Strano, J. N. Coleman, *Science* **2013**, *340*, 1226419.
- [3] J. W. Colson, W. R. Dichtel, *Nat. Chem.* **2013**, *5*, 453.
- [4] H. P. Cong, J. F. Chen, S. H. Yu, *Chem. Soc. Rev.* **2014**, *43*, 7295.
- [5] R. Ma, T. Sasaki, *Acc. Chem. Res.* **2015**, *48*, 136.
- [6] M. Osada, T. Sasaki, *J. Mater. Chem.* **2009**, *19*, 2503.
- [7] Q. Wang, D. O'Hare, *Chem. Rev.* **2012**, *112*, 4124.
- [8] A. Ambrosi, M. Pumera, *Chem. Soc. Rev.* **2018**, *47*, 7213.
- [9] Z. Sun, Q. Fan, M. Zhang, S. Liu, H. Tao, J. Texter, *Adv. Sci.* **2019**, *6*, 1901084.
- [10] C. Tirayaphanitchkul, K. Imwiset, M. Ogawa, *Bull. Chem. Soc. Jpn.* **2021**, *94*, 678.
- [11] Y. Oaki, *Chem. Lett.* **2021**, *50*, 305.
- [12] T. Kato, N. Mizoshita, K. Kishimoto, *Angew. Chem., Int. Ed.* **2006**, *45*, 38.
- [13] K. Ariga, O. Ji, J. P. Hill, A. Vinu, *Soft Matter* **2009**, *5*, 3562.
- [14] J. Broer, C. M. W. Bastiaansen, M. G. Debije, A. P. H. J. Schenning, *Angew. Chem., Int. Ed.* **2012**, *51*, 7102.
- [15] T. Govindaraju, M. B. Avinash, *Nanoscale* **2012**, *4*, 6102.
- [16] T. Kato, M. Gupta, D. Yamaguchi, K. P. Gan, M. Nakayama, *Bull. Chem. Soc. Jpn.* **2021**, *94*, 357.
- [17] A. W. Coleman, S. G. Bott, S. D. Morley, C. M. Means, K. D. Robinson, H. Zhang, J. L. Atwood, *Angew. Chem., Int. Ed.* **1988**, *27*, 1361.

- [18] A. Matsumoto, T. Odani, T. Sada, M. Miyata, K. Tashiro, *Nature* **2000**, 405, 328.
- [19] Y. Ishijima, H. Imai, Y. Oaki, *Chem* **2017**, 3, 509.
- [20] H. Terada, H. Imai, Y. Oaki, *Adv. Mater.* **2018**, 30, 1801121.
- [21] X. Zhuang, Y. Mai, D. Wu, F. Zhang, X. Feng, *Adv. Mater.* **2015**, 27, 403.
- [22] J. Wang, N. Li, W. Xu, H. Pang, *Chem. - Eur. J.* **2020**, 26, 6402.
- [23] Y. Tao, W. Ji, X. Ding, B. H. Han, *J. Mater. Chem.* **2021**, 12, 7336.
- [24] U. Khan, A. Nairan, J. Gao, Q. Zhang, *Small Struct.* **2023**, 4, 2200109.
- [25] S. Okada, S. Peng, W. Spevak, D. Charych, *Acc. Chem. Res.* **1998**, 31, 229.
- [26] M. A. Reppy, B. Piindzola, *Chem. Commun.* **2007**, 42, 4317.
- [27] D. J. Ahn, S. Lee, J. M. Kim, *Adv. Funct. Mater.* **2009**, 19, 1483.
- [28] R. Jelinek, M. Ritenberg, *RSC Adv.* **2013**, 3, 21192.
- [29] D. H. Park, B. J. Park, J. M. Kim, *Acc. Chem. Res.* **2016**, 49, 1211.
- [30] X. Qian, B. Städler, *Chem. Mater.* **2019**, 31, 1196.
- [31] Y. Oaki, *Chem. Commun.* **2020**, 56, 13069.
- [32] M. Weston, A. D. Tjandra, R. Chandrawati, *Polym. Chem.* **2020**, 11, 166.
- [33] B. Das, S. Jo, J. Zheng, J. Chen, K. Sugihara, *Nanoscale* **2022**, 14, 1670.
- [34] B. Tieke, G. Lieser, G. Wegner, *J. Polym. Sci., Polym. Chem. Ed.* **1979**, 17, 1631.
- [35] I. S. Park, H. J. Park, J. M. Kim, *ACS Appl. Mater. Interface* **2013**, 5, 8805.
- [36] D. H. Park, B. J. Park, J. M. Kim, *Acc. Chem. Res.* **2016**, 49, 1211.
- [37] B. Kim, M. I. Khazi, J. M. Kim, *Macromolecules* **2021**, 54, 8220.
- [38] M. Nakamitsu, H. Imai, Y. Oaki, *ACS Sens.* **2020**, 5, 133.
- [39] M. Nakamitsu, K. Oyama, H. Imai, S. Fujii, Y. Oaki, *Adv. Mater.* **2021**, 33, 2008755.
- [40] A. Edagawa, S. Matsuda, H. Kawakubo, H. Imai, Y. Oaki, *ACS Appl. Mater. Interface* **2022**, 14, 43792.
- [41] Y. Ishijima, M. Okaniwa, H. Imai, Y. Oaki, *Chem. Sci.* **2017**, 8, 647.
- [42] B. Hu, S. Sun, B. Wu, P. Wu, *Small* **2019**, 15, 1804975.
- [43] B. Hu, P. Wu, *Giant* **2020**, 3, 100025.
- [44] D. Jang, J.-M. Heo, F. Jannah, M. I. Khazi, Y. Son, J. Noh, H. An, S. Park, D. Yoon, N. N. Kadamannil, R. Jelinek, J. M. Kim, *Angew. Chem., Int. Ed.* **2022**, 61, e202211465.
- [45] J. M. Heo, Y. Kim, S. Han, J. F. Joung, S. H. Lee, S. Han, J. Noh, J. Kim, S. Park, H. Lee, Y. M. Choi, Y. S. Jung, J. M. Kim, *Macromolecules* **2017**, 50, 900.
- [46] J. M. Heo, Y. Son, S. Han, H. J. Ro, S. Jun, U. Kundapur, J. Noh, J. M. Kim, *Macromolecules* **2019**, 52, 4405.
- [47] N. Shioda, J. M. Heo, B. Kim, H. Imai, J. M. Kim, Y. Oaki, *Sens. Diagn.* **2022**, 1, 160.
- [48] K. Bae, J. M. Heo, M. I. Khazi, J. F. Joung, S. Park, Y. Kim, J. M. Kim, *Cryst. Growth Des.* **2020**, 30, 434.
- [49] N. N. Kadamannil, J. M. Heo, D. Jang, R. Zalk, S. Kolusheva, R. Zarivach, G. A. Grank, J. M. Kim, R. Jelinek, *J. Am. Chem. Soc.* **2022**, 144, 17889.
- [50] T. Sasaki, M. Watanabe, H. Hashizume, H. Yamada, H. Nakazawa, *J. Am. Chem. Soc.* **1996**, 118, 8329.
- [51] T. Sasaki, M. Watanabe, *J. Am. Chem. Soc.* **1998**, 120, 4682.
- [52] J. S. Filhol, J. Deschamps, S. G. Dutremez, B. Boury, T. Barisien, L. Legr, M. Schott, *J. Am. Chem. Soc.* **2009**, 131, 6976.
- [53] J. S. Sears, R. R. Chance, J. L. Brédas, *J. Am. Chem. Soc.* **2010**, 132, 13313.
- [54] K. Haraguchi, T. Takehisa, *Adv. Mater.* **2002**, 14, 1120.
- [55] L. Z. Zhao, C. H. Zhou, J. Wang, D. S. Tong, W. H. Yu, H. Wang, *Soft Matter* **2015**, 11, 9229.